



Tolerant, broadband tunable 2×2 coupler circuit

MI WANG,^{1,2}  ANTONIO RIBERO,^{1,2} YUFEI XING,^{1,2}  AND WIM BOGAERTS^{1,2,*} 

¹*Ghent University - imec, Photonic Research Group, Department of Information Technology, Ghent, Belgium*

²*Center of Nano and Biophotonics, Ghent University, Belgium*

*wim.bogaerts@ugent.be

Abstract: We propose a circuit design for a broadband tunable 2×2 waveguide coupler, consisting of a two-stage Mach-Zehnder interferometer with electro-optic phase shifters in each stage. We demonstrate that such design can be configured as a tunable coupler with arbitrary coupling ratio and with a uniform response over 50-nm spectral range around 1550 nm. The design is also tolerant to fabrication variations that affect the coupling ratios of the directional couplers.

© 2020 Optical Society of America under the terms of the [OSA Open Access Publishing Agreement](#)

1. Introduction

Photonic integrated circuits (PIC) integrate multiple optical functions on a chip, similar as in an electronic integrated circuit. Applications of these PICs lay in fields such as telecommunication, quantum computing and so on. One of the essential building blocks for these optical circuits is a 2×2 waveguide coupler, the integrated equivalent of an optical beam splitter. Such component is essential for power distribution as well as the construction of interferometric wavelength filters [1,2].

It is preferable that these couplers have a broadband response, especially for applications such as linear transformations, switch fabrics or bandpass filters. Also, tunability is another property that is highly desirable, as it can make photonic circuits more flexible, up to the point where we can make programmable photonic circuits where many waveguides are connected in a mesh with tunable 2×2 couplers [3].

Nowadays, a 2×2 coupler is normally implemented as an MMI (multimode interference meter) or a directional coupler. An MMI can be made broadband and quite tolerant to fabrication variations, but is hard to engineer for arbitrary coupling ratios, and it is not easily tunable. A directional coupler has been widely used as a power coupler in the silicon-on-insulator (SOI) platform due to the ease of fabrication. However the tolerance to fabrication variation and the wavelength independence are insufficient.

A directional coupler is a wavelength dependent device, especially in high-contrast materials like silicon [4]. Directional couplers which have been engineered to have a broadband response are usually designed for a fixed splitting ratio (e.g. 50:50) [5].

Normally, a tunable coupler made with single-stage Mach-Zehnder interferometer (MZI) would require an ideal 50:50 splitters/combiners to achieve 0-100% splitting ratio [6]. However, due to fabrication variation, the fabricated device (e.g. 50:50 splitters/combiners) will deviate from the designed value, and this will limit the coupling range that can be addressed with the MZI circuit. Also, as the directional couplers are wavelength dependent, the coupling of the MZI circuit will also be wavelength dependent.

Therefore, a fabrication-tolerant 2×2 coupler circuit, that can be tuned from 0 to 100% coupling, and this over a wide wavelength range, is a highly needed building block to construct complex circuits.

In order to address this issue, Miller has proposed a three-stage MZI circuit, which we could also call a $2 \times 2 \times 2 \times 2$ MZI design [6]. This can be seen as a regular single-stage 2×2 MZI where the two directional couplers (splitter and combiner) have been replaced by a tunable 2×2 MZI circuit, thereby guaranteeing that a 50:50 coupling can be obtained in both the splitter and combiner. Suzuki has also proposed a reduced two-stage design (a $2 \times 2 \times 2$ MZI) [7], however neither of these designs address the issue of wavelength dependence.

In this paper, we are building on the two-stage $2 \times 2 \times 2$ MZI design and explore its use and configuration for a broadband coupling response. As we will show, optimizing the device performance is as much about the control as well as about the device design itself. This paper is organized as follows. Section 2 explains the basic principle and tolerance of the design, while section 3 presents an underlying theoretical description. Section 4 and section 5 present the simulation and experimental results. The real-time optimization algorithm is explained in section 6. Section 7 concludes the paper.

2. Tolerant tunable 2×2 coupler

Due to fabrication variations, a fabricated device will always deviate from its designed performance. For example, a 3dB 2×2 coupler, either implemented as a directional coupler or a multimode interferometer, can easily suffer from a few percent points of coupling variation from the ideal 50:50 splitting ratio at 1550 nm. Thus, tolerant designs that compensate for these variations in the optical circuits are very much desired, but not easily implemented.

The typical implementation for a tunable coupler is a balanced MZI. The MZI is constructed with two static 50:50 couplers such as directional couplers (DCs), connected with two waveguides with integrated phase shifters (e.g. heaters). The power transmissions in both outputs ('bar' and 'cross') cover the whole range of 0% to 100% only when the splitter and combiner have a perfect 3dB (50:50) splitting ratio. When the coupling ratio of the directional couplers deviates from its designed value, the power coupling range in 'cross' will not go all the way to 100%, and the bar transmission can not be suppressed all the way down to 0%.

And as already mentioned, even if the directional couplers have a perfect 50:50 splitting ratio, this is usually only the case for a narrow wavelength range, as the directional couplers are wavelength dependent. Alternative couplers, such as MMIs [8] and phase-compensated directional couplers [5] offer a more broadband 50:50 coupler, but these can also suffer from deviations due to fabrication variability.

The accumulation of imperfections caused by fabrication variation would have huge impact on large programmable circuits with hundreds or thousands of tunable couplers, especially on functions that rely on 'cross' coupling with a very high rejection ratio in the 'bar' port. In order to solve this issue, Miller [6] has proposed the following structure as the tolerant design for the tunable coupler. Basically, each directional coupler in the single stage MZI has been replaced with a balanced MZI, as illustrated in Fig. 1(a). This results in a circuit with 3 concatenated MZI stages, each with tunable phase delay in the arms. As long as the directional couplers in the design have a coupling ratio between 85:15 to 15:85, the circuit can be tuned to achieve transmission from 0 to 100%. However, such design would require control electronics for at least 3 heaters.

To reduce the control complexity, we propose a similar circuit with only two tunable MZI stages (three directional couplers with two thermal tuners), similar to what has been proposed in [7], as shown in Fig. 1(b). The coupler circuit can be tuned from 0% to 100% as long as the three directional couplers have a balance that is better than 25:75, which is shown in Fig. 2. Compared to the three-stage design, the tuning algorithm becomes simpler while it is still tolerant to fabrication imperfections and even local variability.

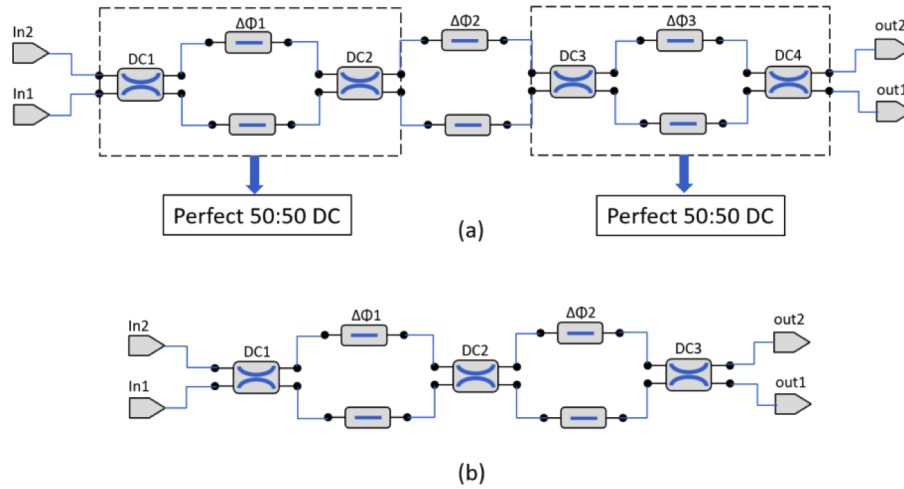


Fig. 1. (a) Three-stage design for the tolerant tunable coupler, as proposed by Miller [6]. (b) Circuit schematic of the two-stage broadband tunable coupler [7]. The directional couplers (DCs) are connected with two waveguides with integrated phase shifters (e.g. heaters), which correspond to the phase compensation section $\Delta\phi_1$ and $\Delta\phi_2$.

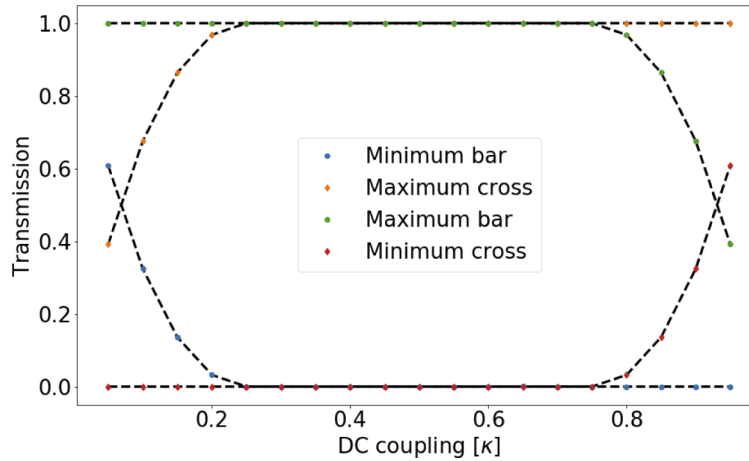


Fig. 2. Addressable range of the transmission curve for Fig. 1(b) for different values of the DC coupling k . We set the coupling of all DCs k_i to be same, and calculated the minimum and maximum transmission in both bar and cross coupling. We see that, as long as the DCs have coupling values between 0.25 to 0.75, we are able to achieve transmission between 0% and 100%.

3. Theoretical analysis

To understand how we can turn the two-stage $2 \times 2 \times 2$ MZI in Fig. 1(b) into a tolerant, but also a broadband tunable coupler, we built a simple analytical model of this circuit, using the transfer matrix method (TMM). The complex amplitudes of the input and output electromagnetic waves have the following relationship between each other:

$$\begin{bmatrix} E_{out1} \\ E_{out2} \end{bmatrix} = C_3 \times P_2 \times C_2 \times P_1 \times C_1 \times \begin{bmatrix} E_{in1} \\ E_{in2} \end{bmatrix} \quad (1)$$

where E_{in1} and E_{in2} are the complex amplitudes of the light in the fundamental waveguide modes at the inputs and E_{out1} and E_{out2} represent the same quantities at the outputs for the 2×2 device. Matrix C_i is the coupling matrix of each directional coupler and Matrix P_i is the propagation matrix of a phase delay section (consisting of two parallel waveguides or phase shifters) for the single stage MZI. The coupling matrix, C_i , is given by:

$$C_i = \begin{bmatrix} \sqrt{1-k_i} & -j\sqrt{k_i} \\ -j\sqrt{k_i} & \sqrt{1-k_i} \end{bmatrix} \quad (2)$$

where k_i is the power cross-coupling coefficient, and $1 - k_i$ is the straight-through coefficient for the directional coupler. Note that the value of k_i can be different for each directional coupler, and it is also wavelength dependent, and sensitive to fabrication variations. For the rest of the derivation, we assume that $k_1 = k_2 = k_3 = k$, but this does not affect the general conclusions.

The propagation matrix P_i of each phase delay section is given by:

$$P_i = \begin{bmatrix} e^{-j\phi_i} & 0 \\ 0 & 1 \end{bmatrix}, \quad (3)$$

where we assume no loss, and equal length for waveguide propagation, so the common propagation terms can be ignored.

The final transfer matrix can then be derived as:

$$\begin{aligned} T_{11} &= \sqrt{1-k}(-k(e^{j\phi_1} + 1)e^{j(\phi_1+\phi_2)} + (-ke^{j\phi_1} - k + 1)e^{j\phi_1})e^{-j(2\phi_1+\phi_2)} \\ T_{21} &= j\sqrt{k}(k-1)(e^{j\phi_1} + 1)e^{j\phi_1} + (k + (k-1)e^{j\phi_1})e^{j(\phi_1+\phi_2)}e^{-j(2\phi_1+\phi_2)} \end{aligned} \quad (4)$$

T_{11} is the transfer function of the bar port of the $2 \times 2 \times 2$ MZI, while T_{21} is the cross transmission. In order to have the broadband response of the device for a certain coupling ratio k of the tunable couplers, two conditions need to be satisfied:

- The dispersion of the power transmission $\int_{\lambda_1}^{\lambda_2} \frac{\partial |T_{11}(\lambda)|^2}{\partial \lambda} d\lambda \rightarrow 0$
- $|T_{11}|^2 = \text{desired coupling ratio } K$

We can rewrite the dispersion for the bar port $\frac{\partial |T_{11}(\lambda)|^2}{\partial \lambda}$ as:

$$\frac{\partial |T_{11}(\lambda)|^2}{\partial \lambda} = \frac{\partial |T_{11}(k)|^2}{\partial k} \cdot \frac{\partial k(\lambda)}{\partial \lambda} \quad (5)$$

We can describe the wavelength dependence of the directional coupler as a Taylor polynomial expansion around the center wavelength λ_0 :

$$k(\lambda) = k_0 + k' \cdot (\lambda - \lambda_0) + \frac{k''}{2} \cdot (\lambda - \lambda_0)^2 + \dots \quad (6)$$

Now the first-order derivative at λ_0 becomes

$$\frac{\partial k(\lambda)}{\partial \lambda} = k' \quad (7)$$

k' is the first order derivative of k , and in order to make the tunable coupler as broadband as possible, we could try to reduce k' by engineering the directional coupler to make it less

wavelength dependent according to Eq. (5). This requires a physical optimization. Instead, we can choose not to engineer k' , but use the phases ϕ_1 and ϕ_2 to compensate for k' . Squaring and deriving (4) gives us:

$$\begin{aligned} \frac{\partial |T_{11}(k)|^2}{\partial k} = & (1 - 3k^2 + 4k)e^{j\phi_1 + j\phi_2} + (1 - 3k^2 + 4k)e^{-j\phi_1 - j\phi_2} + \\ & (2k - 3k^2)e^{-j\phi_1 + j\phi_2} + (2k - 3k^2)e^{j\phi_1 - j\phi_2} + \\ & (1 - 6k^2 + 6k)e^{j\phi_1} + (1 - 6k^2 + 6k)e^{j\phi_2} + \\ & (1 - 6k^2 + 6k)e^{-j\phi_1} + (1 - 6k^2 + 6k)e^{-j\phi_2} \end{aligned} \quad (8)$$

If we use second order polynomials and neglect higher-order terms, the 3dB directional coupler given by Fig. 3(c) could be simplified as $k = k_0 + k' \cdot (\lambda - \lambda_0)$, where the desired power coupling $K = 0.5$ for $\lambda_0 = 1550 \text{ nm}$. We find that $k(\lambda_1) = 0.75$ and $k(\lambda_2) = 0.15$ are corresponding coupling ratios of the DC at wavelengths $\lambda_1 = 1525 \text{ nm}$ and $\lambda_2 = 1575 \text{ nm}$. For the $2 \times 2 \times 2$ MZI with a dispersive 3dB directional coupler in wavelength range $[\lambda_1, \lambda_2]$, the dispersion $\int_{\lambda_1}^{\lambda_2} \frac{\partial |T_{11}(\lambda)|^2}{\partial \lambda} d\lambda$ could be simplified to:

$$\begin{aligned} \int_{\lambda_1}^{\lambda_2} \frac{\partial |T_{11}(\lambda)|^2}{\partial \lambda} d\lambda &= \int_{\lambda_1}^{\lambda_2} \frac{\partial |T_{11}(k)|^2}{\partial k} \cdot \frac{\partial k(\lambda)}{\partial \lambda} d\lambda = \int_{k(\lambda_1)}^{k(\lambda_2)} \frac{\partial |T_{11}(k)|^2}{\partial k} \cdot dk \\ &= ((k - k^3 + 2k^2)(e^{j\phi_1 + j\phi_2} + e^{-j\phi_1 - j\phi_2}) + (k^2 - k^3)(e^{-j\phi_1 + j\phi_2} + e^{j\phi_1 - j\phi_2}) + \\ &\quad (k - 2k^3 + 3k^2)(e^{j\phi_1} + e^{j\phi_2} + e^{-j\phi_1} + e^{-j\phi_2})) \Big|_{k(\lambda_1)}^{k(\lambda_2)} \\ &= -0.0615(e^{j\phi_1 + j\phi_2} + e^{-j\phi_1 - j\phi_2}) - 0.1215(e^{-j\phi_1 + j\phi_2} + e^{j\phi_1 - j\phi_2}) - \\ &\quad 0.183(e^{j\phi_1} + e^{j\phi_2} + e^{-j\phi_1} + e^{-j\phi_2}) \end{aligned} \quad (9)$$

The basic principle of configuring a two-stage MZI as a broadband coupler is explained in Fig. 3. The grey region in Fig. 3(a) is the region with less than 5% dispersion over 50 nm wavelength range in central wavelength 1550 nm according to Eq. (9).

Figure 3(b) is the coupling plot for the central wavelength $\lambda_0 = 1550 \text{ nm}$. The broadband response for different coupling ratios lies in the region which is the combination of grey region in Fig. 3(a) and contour lines of Fig. 3(b) in the 2D phase space $(\phi_1$ and $\phi_2)$. Figure 3(c) is the spectrum response of the 50:50 DC used in our fabricated device. It is clear that the DC only has good 50:50 coupling around $\lambda_0 = 1550 \text{ nm}$. The DC is wavelength dependent, and the measured coupling values for different wavelengths are used in the simulation of Fig. 3(d).

Figure 3(d) is the simulation result for the same cross coupling points in the 2D phase space of (ϕ_1, ϕ_2) . For any coupling ratio, there are a number of phase combinations that will give the correct coupling, which corresponds to the contour lines in Fig. 3(d). However for different wavelengths, these contours become distorted, because the directional couplers have different coupling strength at other wavelengths. The change in coupling strength can be compensated by the control of the constructive/destructive interference through the two phase shifters. The region in the 2D phase space indicated by the red dotted line, where the contours for different wavelengths are intersecting, is indicative of a broadband operating regime over a wavelength range of 50 nm. Essentially, this configuration of (ϕ_1, ϕ_2) results in an region where the contours of different wavelengths intersect or come very close together.

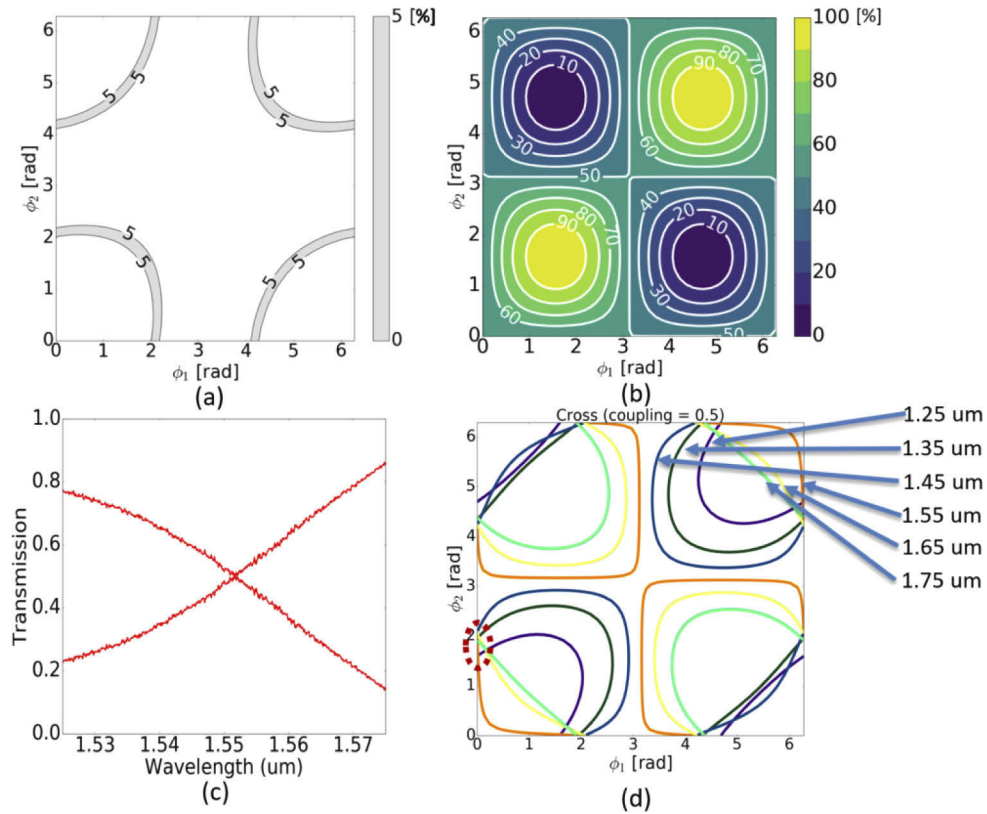


Fig. 3. (a) Iso-contours for the wavelength dispersion given by Eq. (9), where λ_1 is 1525 nm, λ_2 is 1575 nm. We normalize the absolute value of the dispersion; the grey region indicates settings with less than 5% dispersion. (b) plots the cross transmission at 1550 nm. (c) The spectrum response of a single 50:50 DC used in our fabricated device. (d) The (ϕ_1, ϕ_2) contour to obtain a coupling ratio of 0.5 for different wavelengths has been plotted based on Eq. (8). The region in the 2D phase space indicated by the red dotted line, where the contours for different wavelengths are intersecting, is indicative of a broadband operating regime over a wavelength range of 50 nm.

4. Tuning for broadband operation

Based on this model, we understand that we can configure the $2 \times 2 \times 2$ MZI as a wavelength-independent tunable coupler, which is very useful for many applications such as wavelength-division multiplexing and signal switching in data communication. However, the coupling ratios of conventional directional couplers are highly sensitive to their operating wavelengths, especially in high-contrast waveguide materials such as silicon. A broadband 2×2 coupler would have the desired response that the coupling ratio remains the same in a larger bandwidth.

Figure 4 presents the simulation of a two-stage tunable coupler with directional couplers with a perfect 50:50 splitting ratio at 1550 nm, the model for 3dB directional coupler has been explained in section 3. Figure 4(a) is the cross transmission at a wavelength of 1550 nm, Fig. 4(b) is the maximum deviation of the cross coupling between 1525 nm and 1575 nm for the two-stage tunable coupler. The dark regions bounded by the yellow contours in the graph indicate the region of 3% deviation from the desired coupling within a 50 nm wavelength range around 1550 nm. Figure 4(c) is the transmission spectra of the corresponding points in Fig. 4(b): only point 2 and 4 have a flat spectral response, corresponding to the dark region in Fig. 4(b). Figure 4(d) is

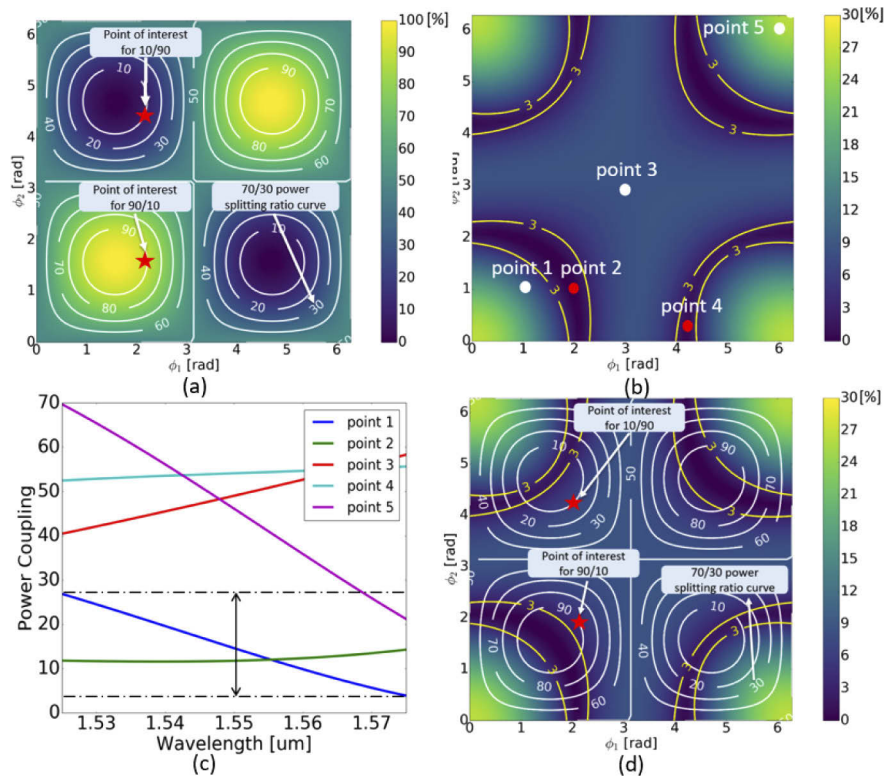


Fig. 4. Simulations of a two-stage MZI tunable coupler with a directional coupler with a perfect 50:50 splitting ratio at 1550 nm. (a) Cross transmission at a wavelength of 1550 nm. (b) Maximum deviation of the cross coupling between 1525 nm and 1575 nm for the two-stage tunable coupler. (c) Transmission spectra of the corresponding points in (b). (d) Combination of (a) and (b).

the combination of Fig. 4(a) and Fig. 4(b): the dark region contains the entire 0-100% coupling range, so we can use the circuit as a 50 nm broadband tunable coupler with only 3% coupling tolerance.

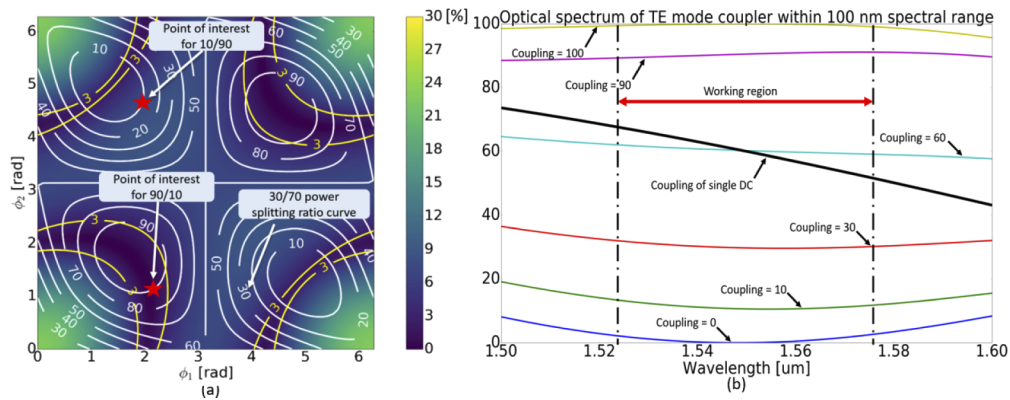


Fig. 5. Simulation result of a two-stage tunable coupler with imperfect DCs with a 40:60 coupling ratio at wavelength 1550 nm. (a) corresponds to Fig. 4(d), (b) is the simulated cross power transmission for 0%, 10%, 40%, 70%, 90% and 100% coupling ratio.

Similarly, Fig. 5 shows the simulation result of the same two-stage tunable coupler, but with imperfect DCs of 40:60 coupling ratio at 1550 nm. The simulation result showed that such design could also work as a tunable coupler with any coupling ratio in 50 nm wavelength range of central wavelength 1550 nm, which means that the two stage tunable coupler design is tolerant to fabrication variations according to simulation. In Fig. 5(b), within the working region between 1525 nm and 1575 nm indicated by the dashed line, the device works as a broadband coupler with a deviation less than 3%. Outside this working region, the coupler suffers more wavelength dispersion. The dispersive response of a single DC with 40:60 coupling ratio at 1550nm is also shown by black bold line. Such design also works when the three directional couplers have different coupling values, as long as they are within the safe zone of 25:75 as illustrated in Fig. 2.

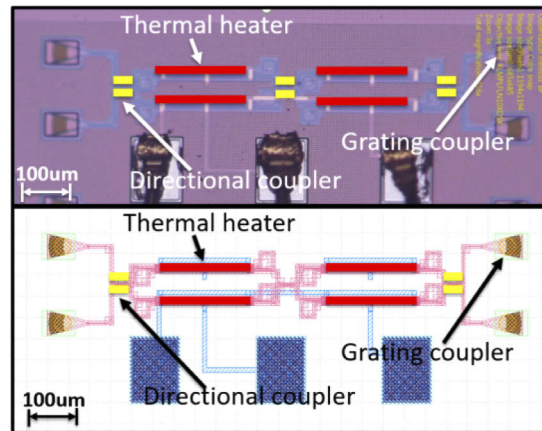


Fig. 6. Fabricated chip on the IMEC ISiPP50G platform. (a) microscopic image of the fabricated chip and (b) the corresponding GDS layout of the design.

5. Experimental results

We had this circuit fabricated on IMEC's standard ISiPP50G silicon photonics platform, which we accessed through the Europractice multi-project wafer service. The microscopic image of the chip and the GDS layout have been shown in Fig. 6. In total 3 different designs for the two-stage MZI tunable coupler have been fabricated, with different nominal design values for the directional couplers. Device A has a DC designed with 60:40 split ratio at wavelength 1550 nm, device B with a 65:35 DC, and device C with a 70:30 DC.

The experimental result is compared with simulation. Figure 7 shows both the simulated and experimental transmission for the bar port of device A. The data was measured by sweeping the voltage applied to the thermo-optic phase shifters, which are implemented with a diode in series, as presented in [9]. The sweeping resolution has been chosen to be 0.1 V, and we measured the transmission for 10 wavelength points in the 50 nm wavelength range. Such resolution should be sufficient to see the trend of the spectral response and allows for a good qualitative match between the simulation and experimental results shown in Fig. 7. Figures 7(a) and (b) show the simulation results of the coupling at 1550 nm and the variation over a 50-nm range (both in dB scale). The dark blue region in Fig. 7(b) surrounded by the yellow lines have <1 dB variation, (For a 3 dB coupler, the 1 dB variation region would span from -2 dB to -4 dB. For a -20 dB coupling ratio, the 1 dB region spans from -19 dB to -21 dB.) Figures 7(c) and (d) is the corresponding experimental result, and we can see a good qualitative agreement. The black rectangles in Figs. 7(c) and (d) correspond to the phase space plotted in Figs. 7(a) and (b).

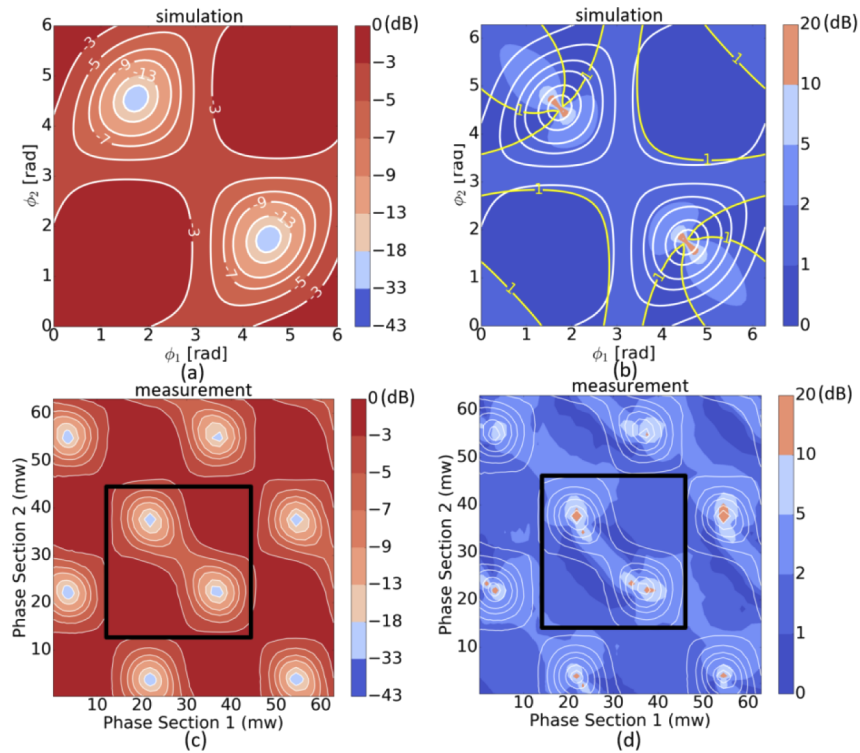


Fig. 7. Comparison between simulation and experiment for device A (50:50). (a) Simulation result of the coupling at a wavelength of 1550 nm on a logarithmic (dB) scale. (b) Variation plot on a logarithmic (dB) scale. (c,d) Corresponding experimental results for (a,b).

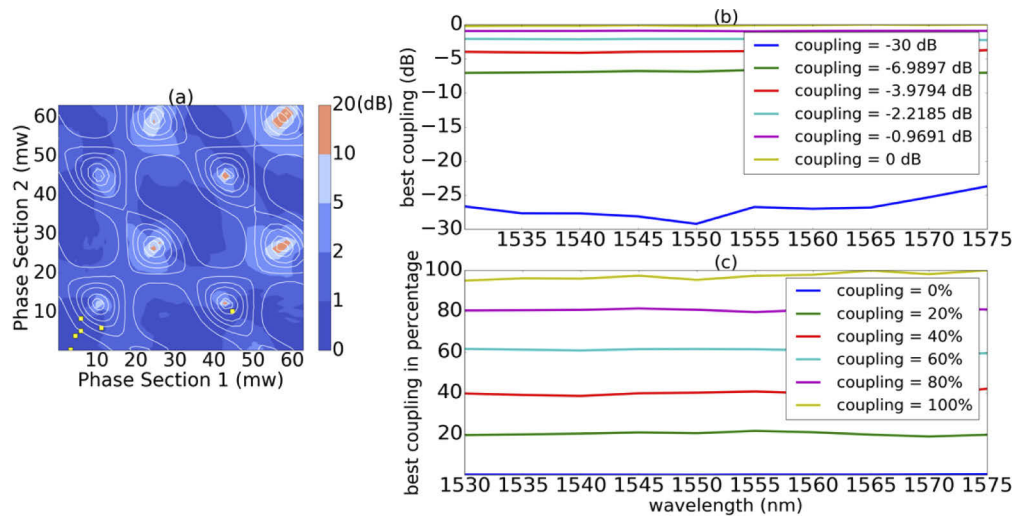


Fig. 8. Similar to Fig. 7(d), the experimental result for the cross port of device B (65:35) is shown in Fig. 8(a), the yellow dots corresponds to coupling values in (b) Coupling values of 0-100% in steps of 20% are plotted using the LUT of Fig. 8(a) in linear scale in Fig. 8(b) and in logarithmic scale in Fig. 8(c).

We can now use the obtained 2-D transmission maps as a look-up table (LUT) for configuring the tunable coupler to search for a desired coupling ratio. This gives us the transmission curves plotted in Fig. 8. We see that the variation for larger coupling ratios are significantly larger than that of smaller coupling ratios.

6. Optimization algorithm

As we can see from the previous section, the performance of the device is also limited by the measurement resolution used to compose the LUT. As the landscape of the LUT is quite smooth, this resolution can be improved through interpolation. As an alternative, we introduce optimization algorithms with control loops to configure the couplers, which enables us to obtain more accurate coupling values in a shorter time. Control loops can be used for all kinds of purposes [9], such as power control, crosstalk minimization [10] and real-time monitoring [11]. As already demonstrated, the LUT provides but a coarse estimation of the driving voltage of the heaters for the desired coupling value. This can be used as a starting point for an optimization algorithm. For coupling optimization at single wavelength, the gradient-descent algorithm [12] is used. For broadband optimisation, we use the Nelder-Mead method [13]. In the following, we will illustrate how these two algorithms work.

6.1. Gradient descent algorithm

The gradient descent algorithm is a first-order iterative optimization algorithm for finding the minimum of a function. In Fig. 9, the gradient descent algorithm is applied in the real-time measurement and the trajectory to get to the maximum and minimum output value is plotted out. The output power measured with power meter is used as input value (x), the model targets to get the best-fit regression to predict the value of y based on x . While training the model, the model calculates the cost function which defined by the Root Mean Squared error between the predicted value ($pred$) and true value (y). The model targets to minimize this cost function [14].

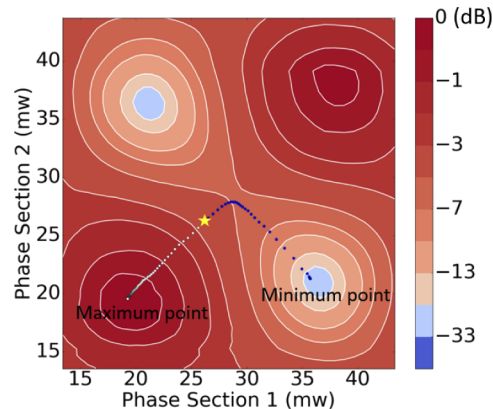


Fig. 9. Experimental result of searching for the maximum and minimum coupling points with gradient descent method.

6.2. Nelder-Mead method

The Nelder-Mead method is a commonly applied numerical method used to find the minimum or maximum of an objective function in a multidimensional space [15]. In real time measurement, the voltages applied to the two phase shifters are used as parameters for optimization. For

broadband operation, we try to minimize the difference between the targeted output spectrum and the real-time measured value. The targeted spectra are the ideal broadband responses of our coupler. By minimizing the cost function similar in Gradient descent method, we could find the best broadband coupling points in the 2-D phase space. In Fig. 8, we already demonstrated the possibility of the device to be configured into a broadband tunable coupler, however in Fig. 10, the broadband coupling response of 40% and 50% have been obtained with the Nelder-Mead method as an example. The transfer spectrum is plotted with 0.1 nm resolution. The oscillations are caused by the resonances of the Fabry-Pérot cavities which are formed by the input and output grating couplers.

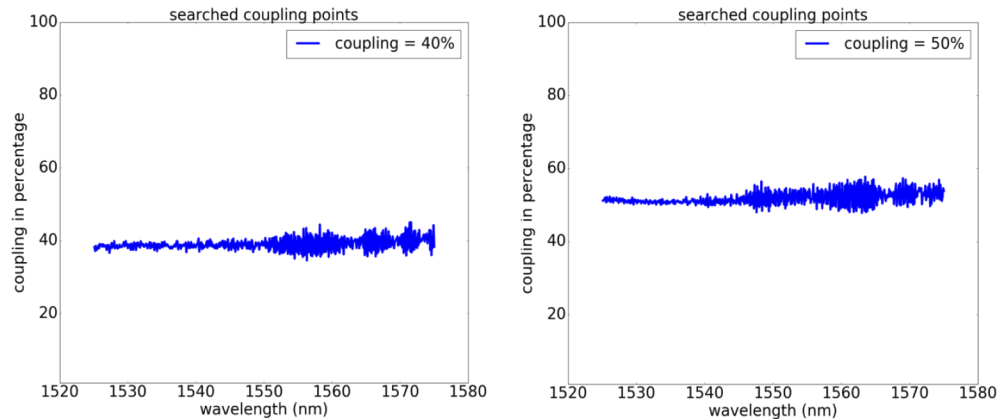


Fig. 10. Experimental result of searching for the broadband coupling value of 40% and 50% using the Nelder-Mead method.

The ripple we observe on the spectrum originates from a cascade of small backreflections which can be attributed to the grating couplers as well as the interfaces of waveguides with the directional couplers and phase shifters. These can be further reduced by optimizing the individual building blocks.

7. Conclusion

We have demonstrated a tolerant design for a broadband tunable coupler, consisting of a two-stage MZI. The coupler can be controlled in a two-dimensional space by adjusting the phase delays in both stages of the MZI. The device is tolerant against variations of the directional couplers, as long as their coupling falls within the range of 25-75%. In addition, we show that, even when the DCs are highly wavelength dependent, the coupler can be configured for wavelength-independent coupling over a wavelength range of 50 nm, and this for all power coupling values from 0% to 100%. The measurement data on the fabricated devices match well with the simulation results. The spectrum variation is demonstrated to be within 5% both in simulation and measurement for the 50 nm wavelength range around 1550 nm for different tunable couplers with intentional variations in the directional couplers. An adaptive tuning algorithm based on the Nelder-Mead method has been tested in real time measurement for configuring the tunable coupler into a broadband coupler.

Funding

European Research Council (PhotonicSWARM (725555)).

Disclosures

The authors declare no conflicts of interest.

References

1. W. Bogaerts, S. K. Selvaraja, P. Dumon, J. Brouckaert, K. De Vos, D. Van Thourhout, and R. Baets, "Silicon-on-insulator spectral filters fabricated with cmos technology," *IEEE J. Sel. Top. Quantum Electron.* **16**(1), 33–44 (2010).
2. W. Bogaerts, P. De Heyn, T. Van Vaerenbergh, K. De Vos, S. Kumar Selvaraja, T. Claes, P. Dumon, P. Bienstman, D. Van Thourhout, and R. Baets, "Silicon microring resonators," *Laser Photonics Rev.* **6**(1), 47–73 (2012).
3. D. Pérez, I. Gasulla, and J. Capmany, "Programmable multifunctional integrated nanophotonics," *Nanophotonics* **7**(8), 1351–1371 (2018).
4. Z. Lu, J. Jhoja, J. Klein, X. Wang, A. Liu, J. Flueckiger, J. Pond, and L. Chrostowski, "Performance prediction for silicon photonics integrated circuits with layout-dependent correlated manufacturing variability," *Opt. Express* **25**(9), 9712–9733 (2017).
5. Z. Lu, H. Yun, Y. Wang, Z. Chen, F. Zhang, N. A. F. Jaeger, and L. Chrostowski, "Broadband silicon photonic directional coupler using asymmetric-waveguide based phase control," *Opt. Express* **23**(3), 3795–3808 (2015).
6. D. A. B. Miller, "Perfect optics with imperfect components," *Optica* **2**(8), 747–750 (2015).
7. K. Suzuki, G. Cong, K. Tanizawa, S.-H. Kim, K. Ikeda, S. Namiki, and H. Kawashima, "Ultra-high-extinction-ratio 2×2 silicon optical switch with variable splitter," *Opt. Express* **23**(7), 9086–9092 (2015).
8. P. A. Besse, M. Bachmann, H. Melchior, L. B. Soldano, and M. K. Smit, "Optical bandwidth and fabrication tolerances of multimode interference couplers," *J. Lightwave Technol.* **12**(6), 1004–1009 (1994).
9. A. Ribeiro, A. Ruocco, L. Vanacker, and W. Bogaerts, "Demonstration of a 4×4 port universal linear circuit," *Optica* **3**(12), 1348–1357 (2016).
10. J. Zeng, D. Sun, X. Liu, X. Cao, B. Yang, N. Wang, D. Liu, and Y. Mu, "Strategy design for controlling on-chip photonic circuits," in *2018 IEEE Student Conference on Electric Machines and Systems*, (IEEE, 2018), pp. 1–6.
11. Y. Huang, Q. Cheng, and K. Bergman, "Advanced control for crosstalk minimization in mzi-based silicon photonic switches," in *2018 IEEE Optical Interconnects Conference (OI)*, (IEEE, 2018), pp. 17–18.
12. J. A. Snyman and D. N. Wilke, *Practical Mathematical Optimization: Basic Optimization Theory and Gradient-based Algorithms*, vol. 133 (Springer, 2018).
13. J. A. Nelder and R. Mead, "A simplex method for function minimization," *Comput. J.* **7**(4), 308–313 (1965).
14. S. Ruder, "An overview of gradient descent optimization algorithms," arXiv preprint arXiv:1609.04747 (2016).
15. M. A. Luersen and R. Le Riche, "Globalized nelder–mead method for engineering optimization," *Comput. Struct.* **82**(23–26), 2251–2260 (2004).